UC Berkeley
SEMM Reports Series

Title

Seismic response of bridges with rocking foundations at a near-fault site

Permalink

https://escholarship.org/uc/item/3w99q5tf

Authors

Antonellis, Grigorios

Panagiotou, Marios

Publication Date

2013-03-01

Report No. UCB/SEMM-2013/04	Structural Engineering Mechanics and Materials

Seismic Response of Bridges with Rocking Foundations at a Near-fault Site

By

Grigorios Antonellis and Marios Panagiotou

| March 2013 | Department of Civil and Environmental Engineering
University of California, Berkeley |

Seismic Response of Bridges with Rocking Foundations at a Near-fault Site

Grigorios Antonellis and Marios Panagiotou

Abstract

This report investigates numerically the three-dimensional seismic response of six reinforced concrete bridges hypothetically located in Oakland, California, 3 km from the Hayward fault. Three of the bridges are 17 m tall and three are 8 m tall. Three types of column-foundation designs are studied: (a) columns that form flexural plastic hinges, which are conventionally designed according to Caltrans seismic design criteria; (b) columns on rocking pile foundations that are designed to remain elastic; and (c) columns designed to remain elastic that are supported on rocking shallow foundations. The bridges with rocking foundations use lead-plug rubber bearings at the abutments to enhance strength, stiffness and hysteretic energy dissipation. Three-dimensional nonlinear response history analyses are performed, using two components of horizontal excitation, for two seismic hazard levels with return periods of 975 and 2475 years, respectively. At both levels of shaking the conventionally designed bridges experience substantial inelastic deformations and damage in the columns, while the bridges with rocking foundations result in essentially elastic response.

Introduction

Conventionally designed bridges rely on the concept of ductility, whereby the column reinforcement is detailed to ensure the development of flexural plastic hinges at the base and the top of the columns. While bridges designed in this manner may be safe from collapse, they are susceptible to considerable damage and permanent lateral displacements that can impair traffic flow and necessitate costly, time consuming, dangerous, and disruptive inspections and repairs. As an alternative design, bridges with columns supported on rocking foundations may develop large nonlinear deformations when subjected to strong shaking but experience far less damage in the columns, with the added bonus of these columns that re-center following a high-intensity earthquake ground motion.

The rocking behavior of structures has been investigated numerically and experimentally since the nineteenth century (Milne and Omori 1893). In 1960 Muto et al. studied the rocking response of slender structures both numerically and through shake table tests, while in 1963 Housner studied numerically the rocking behavior of rigid blocks supported on a rigid base and subjected to ground excitation. Beck and Skinner (1974) conducted the first analytical study to investigate the use of a rocking step pier as an

earthquake-resistant structural system for bridges. This system was later used in the design and construction of the South Rangitikei Railway Bridge, New Zealand (Cormack 1988). Rocking foundations or rocking piers have been utilized in the design (Pecker 2006) and retrofit (Astaneh-Asl and Roberts 1996) of other major bridges or have been proposed for the design and retrofit of bridges (Priestley et al. 1978 and 1996, Pollino and Bruneau 2007).

Over the last four decades, a number of numerical studies of the seismic response of rocking structures have been conducted, including: (1) seismic soil-structure interaction of foundations that uplift (Wolf 1976); (2) rocking flexible structures supported on a flexible base (Chopra and Yim 1985); (3) rigid blocks on a rigid base subjected to pulse-type ground excitation (Makris and Zhang 2001); and, rigid blocks on an inelastic base (Apostolou et al. 2007).

Extensive studies on the numerical investigation of the seismic response of single bridge piers supported on rocking foundations have also been performed, including three-dimensional (3D) (Mergos and Kawashima 2005) and two-dimensional (Deng et al. 2012) response history analysis and use of nonlinear-Winkler-foundation models. Sakellaraki and Kawashima (2006) studied the 3D response of a bridge with columns supported on rocking shallow foundations. This study used a 3D model with fiber section nonlinear beam elements for the columns, nonlinear Winkler-type model for the shallow foundations, elastic beam elements for the deck, springs modeling the behavior of the abutments in the longitudinal direction. In this study a single near-fault ground motion record was used in the 3D analysis of the bridge models.

Some of the first experimental shake table studies of rocking buildings (Kelly and Tsztoo 1977) and of single rocking piers (Priestley et al. 1978) were conducted in the 1970s. Extensive experimental studies of the rocking response of single bridge columns or two-column subassemblies supported on rocking shallow foundations followed, with shake table tests performed by Saidi et al. (2002), Chen et al. (2006), and Espinoza and Mahin (2008). Large-scale experimental studies involving geotechnical aspects of rocking of shallow foundations with static loading (Bartlett 1976; Wiessing 1979; Negro et al. 2000, Paolucci et al. 2007) or dynamic (Paolucci et al. 2007) have also been performed. Finally, numerous centrifuge tests of rocking structures including that of single piers and simple bridge models with columns supported on rocking shallow foundations (Gajan et al. 2005, Deng et al. 2012) and piers supported on rocking pile-foundations (Pecker 2006, Allmond and Kutter 2012) have been performed.

This study investigates the 3D seismic response of bridges with columns supported on rocking foundations and compares their response to that of conventional bridges of similar geometry designed according to current Caltrans Seismic Design Criteria (SDC) (Caltrans 2010). Both rocking shallow foundations and rocking pile foundations are studied. The bridges with rocking foundations use larger diameter lead-plug rubber bearings at the abutments to enhance strength, stiffness, and hysteretic energy dissipation compared to the laminated (no lead-plug) rubber bearings used in the fixed-base bridges. All bridges are located 3 km from the Hayward fault in Oakland, California. Three-dimensional analytical models of the bridges including the foundations, the columns, the deck, and the abutments were developed and subjected to bi-axial horizontal excitation using a set of 14 ground motions scaled to two different seismic hazard levels, with return period equal to 975 and 2475 years, respectively.

Site and Seismic Hazard Description

The bridges in this study are hypothetically located at the intersection of the I-580 and Highway 24, in Oakland, California, 3 km from the Hayward fault, in a site with an average shear wave velocity $V_s = 400$ m / s in the top 30 m of soil. The site seismic hazard and corresponding design spectra were determined (USGS 2013) for two hazard levels: (a) 5% probability of exceedance in 50 years (975-year return period); and (b) 2% probability of exceedance in 50 years (2475-year return period), corresponding to the design earthquake (DE) and maximum considered earthquake (MCE), respectively. Figure 1 shows the design acceleration and displacement spectra at the two seismic hazard levels. Bi-axial horizontal excitation and one set of 14 historical near-fault pulse-like ground motions were used in this 3D numerical study, see Table 1. For each ground motion the fault-normal (FN) and fault-parallel (FP) horizontal component of the original record was used. The vertical component of the ground motions is not used here. The ground motions were linearly scaled such that the average spectrum of the fault-normal components for 5% damping ratio, ζ, matched (approximately) the design spectra at the corresponding hazard level. The corresponding scale factors for each motion are shown in Table 1. For each of the 14 ground motions the same scale factor was applied in the fault-normal and fault-parallel component. The mean acceleration and displacement spectra of the fault-normal components are shown in Figure 1(a), and (b) respectively. The corresponding spectra of the fault-parallel components scaled to the DE are also shown in this figure.
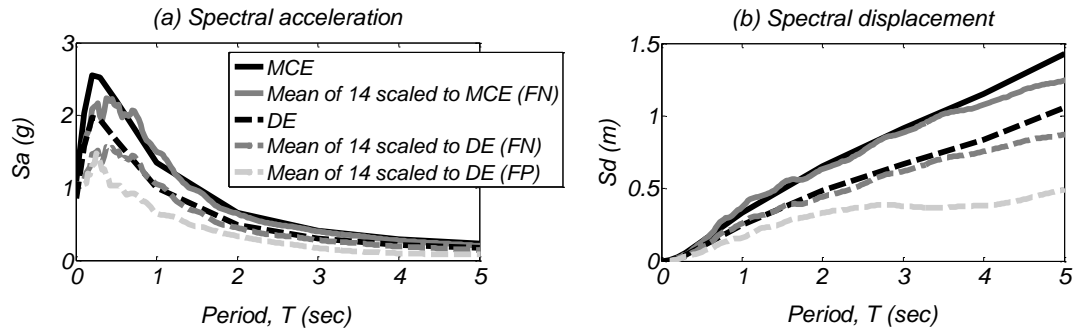
Figure 1. Design linear acceleration and displacement spectra for the DE and MCE seismic hazard levels compared to the corresponding mean spectra at 5% damping ratio, of the 14 ground motions scaled at the corresponding hazard level.

Table 1. Set of the fourteen ground motions and their individual scale factors for the DE and MCE level.

No.	Record	Earthquake name, Location, Year	Scale factors	
			DE	MCE
1	LGPC	Loma Prieta, CA, 1989	1.11	1.58
2	RRS	Northridge, CA, 1994	1.06	1.52
3	TCU052	Chi-Chi, Taiwan, 1999	0.70	1.00
4	PACOIMA DAM	San Fernando, CA, 1971	1.41	2.02
5	NEWHALL	Northridge, CA, 1994	1.31	1.87
6	TABAS	Tabas, Iran, 1978	0.87	1.24
7	DUZCE	Duzce, Turkey, 1999	0.82	1.17
8	ELCEN6	Imperial Valley, CA, 1979	0.42	0.60
9	LUCERNE	Landers, CA, 1992	0.74	1.06
10	TCU074	Chi-Chi, Taiwan, 1999	1.09	1.55
11	CHY028	Chi-Chi, Taiwan, 1999	1.31	1.87
12	SCS	Northridge, CA, 1994	1.10	1.57
13	ELCEN DIFF	Imperial Valley, CA, 1979	0.92	1.32
14	TCU079	Chi-Chi, Taiwan, 1999	1.10	1.57

Description and Design of the Bridges

Figure 2(a) shows a side view of the bridges; Table 2 summarizes the main characteristics. All six bridges had five spans, single column bents, and the deck section shown in Figure 2(b). The height of the bridges, H, is defined as the distance from the ground surface to the top of the deck; see Figure 2(a) and (b). Three designs were investigated in terms of foundation-column design: (1) columns supported on fixed pile foundations and

designed to form flexural plastic hinges at their ends (according to Caltrans SDC), referred to herein as fixed base (FB); (2) columns designed to remain elastic and supported on rocking pile foundations with the pile caps designed to uplift in respect to the piles, referred to herein as rocking pile foundation (RPF); and (3) columns designed to remain elastic supported on shallow foundations designed to uplift in respect to the soil, referred to herein as rocking shallow foundation (RSF). Bridges FB17, RPF17, and RSF17 were 16.5 m tall and bridges FB8, RPF8, and RSF8 were 8 m-tall. The three different designs are discussed in the following three sections. The number after the design description FB, RSF, and RPF refers to the bridge height.

The area of the deck section for all bridges is 6 m^2 and is post-tensioned, with high-strength low-relaxation Grade 270 (ultimate strength $f_{ps,u}$ =1860 MPa) tendons. In all bridges the total area of strands used is A_{ps} = 31080 mm^2 and the initial after losses post-tensioning stress of the strands $f_{ps,i}$ = 1000 MPa (initial strain of strands after losses $\varepsilon_{ps,i}$ = 0.56%). The losses were assumed to be constant along the deck. The deck section has a longitudinal bonded steel ratio of 0.4%. All reinforced concrete components of the six bridges are designed with concrete to a specified compressive strength $f_c^{'}$ = 41 MPa and steel with a specified yield strength of f_y = 413 MPa. The seismic weights, W, given in Table 2 include 3.1 MN live load and three quarters of the weight of the columns.

For the FB bridges the deck at the abutments is supported on two 0.6 m diameter laminated rubber bearings [see Table 2 and Figure 2(c)], consisting of seventeen 12 mm thick rubber layers, with a shear modulus of rubber G_r = 0.6 MPa. For the bridges with rocking foundations the deck at the abutments is supported on two circular laminated 1.26 m diameter lead-plug rubber bearings (LPRB), consisting of twenty six 12 mm thick rubber layers with G_r = 0.6 MPa, and a 340 mm lead-plug with shear modulus of lead G_L = 150 MPa and yield stress of lead τ_L = 10 MPa. The shear keys of the abutments in the transverse direction are the same for all six bridges and designed to have a lateral strength of 660 kN. The expansion joints at the abutments are identical for all six bridges and have a deformation capacity of 0.10 m; see Figure 2(d). The next three sections describe each of the column-foundation designs.
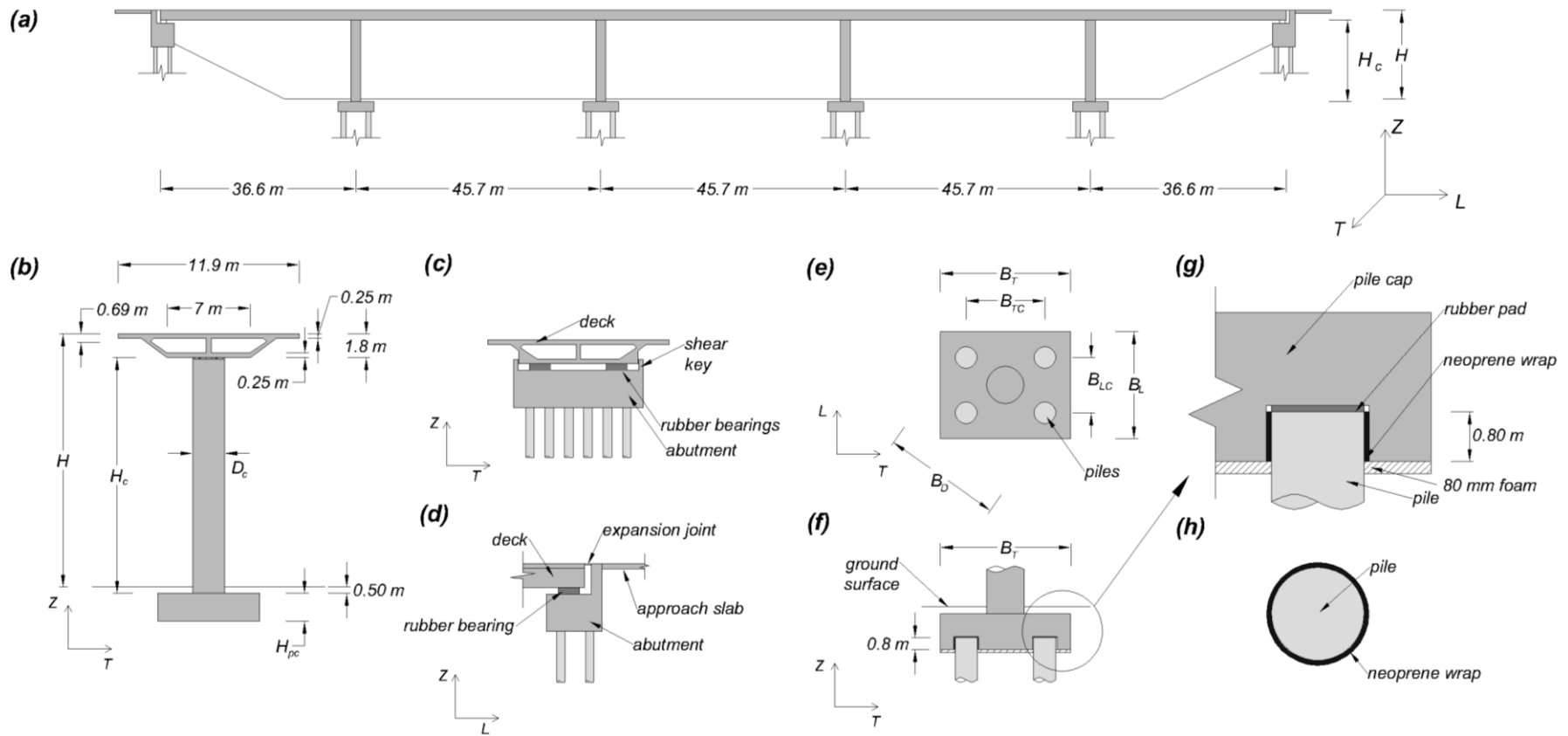
Figure 2. Geometric characteristics of the bridges: (a) side view of the whole bridge; (b) elevation view of the foundation-column and deck of bridge RSF17; (c) elevation section view of abutment, bearings, and deck of the bridges; (d) side elevation view of abutment, bearing, deck and expansion joint of all bridges; (e) plan view of the pile foundations; (f) elevation section view of the rocking pile foundations; (g) elevation section view of pile cap to pile connection of the rocking pile foundations; and (h) section view of pile and neoprene wrap of the rocking pile-foundations.

Table 2. Main characteristics of the six bridges.

Bridge name		FB17	FB8	RPF17	RPF8	RSF17	RSF8
Type of foundation		Fixed pile foundation		Rocking pile foundation		Rocking shallow foundation	
Seismic weight above ground, W (MN)		47.7	46.1	50.2	47.2	50.2	47.2
Foundation	Height of pile cap or of shallow found., H_{pc} (m)	2.0		2.4	2.4	2.0	
	Width B_T (m) / B_{TC} (m)	7.0 / 3.8		8.8 / 5.3	8.5 / 5.0	8.0	
	Length B_L (m) / B_{LC} (m)	7.0 / 3.8		7.2 / 3.7	7.0 / 3.5	8.0	
	Number of piles	4		4		N/A	
	Pile diameter (m) / Pile length (m)	1.5 / 20		1.5 / 25		N/A	
Column	Height, H_c (m)	15.2	6.7	15.2	6.7	15.2	6.7
	Diameter, D_c (m)	1.8	1.8	2.5	2.5	2.5	2.5
	Base axial force interior col., (MN)	10.6	10.3	11.1	10.4	11.2	10.4
	Long. reinforcing steel ratio, ρ_l (%)	2	2	3	3	3	3
	Connection with deck	Fixed	Fixed	Pin	Pin	Pin	Pin
Bearing	Diameter (m)	0.6		1.26			
	Total height of rubber, t_r (mm)	200		312			
	Diameter of lead plug (m)	N/A		0.34			

Fixed-base (FB) bridges

In general, the majority of inelastic deformations in these bridges are expected to develop in flexural plastic hinges near the two ends of the columns, especially near the base. For the FB bridges the columns were designed to be fixed at both ends. Figure 3 shows the expected deformation pattern of the FB bridges responding in the transverse direction. These bridges are designed based on the Caltrans SDC (2010). The column diameter for bridges FB17 and FB8 is 1.8 m and have longitudinal steel ratio $\rho_l = 2\%$. Based on the moment-curvature section analysis using expected material properties (described in section *Numerical Model*), the flexural strength of the columns at 1%, and 5% tensile strain of the longitudinal reinforcement and for axial compression force equal to 10.6 MN was computed equal to 24.8 MN-m, and 28.1 MN-m, respectively. The FB bridges use a pile-foundation for the columns with a 7 m square and 2 m deep pile cap fixed to 4 RC piles, each pile being 1.5 m in diameter and 20 m long.
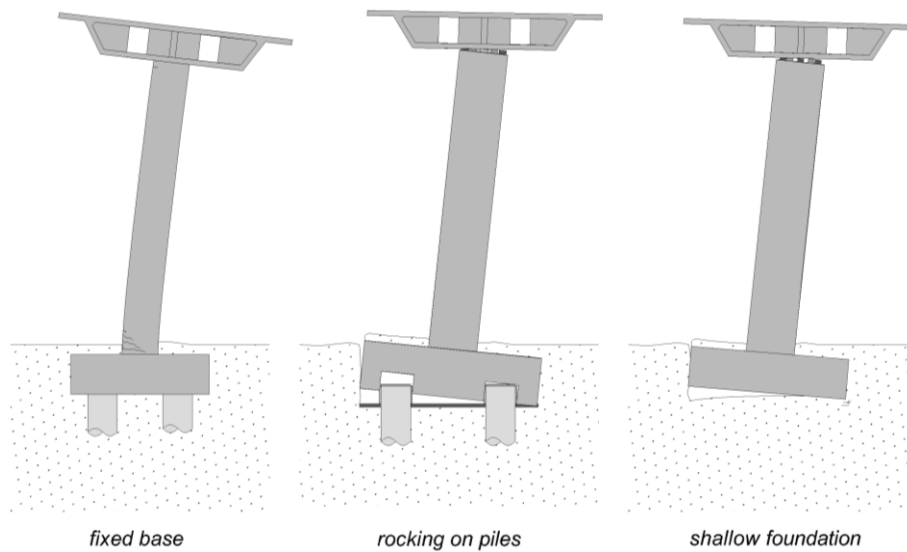
Figure 3. Schematic of foundation, column and deck in a deformed state at a 5% transverse drift ratio for the three designs studied (displacements are drawn magnified by 2).

Bridges with rocking pile foundations (RPF)

The majority of deformations in the bridges with a RPF are due to rocking of the pile cap with respect to the piles, see Figure 3; the deck, columns, pile cap, and piles are designed to remain nominally elastic at the MCE level of shaking without exceeding 5% drift ratio and 0.5% residual drift ratio; This design is used in lieu of a RSF design because the soil properties near the ground surface are such that they cannot achieve the above design objectives.

In the RPF design the rectangular pile cap is simply seated on top of four 1.5 m diameter RC piles, which protrude into the pile cap [see Figure 2 (e), (f) and (g)], and is practically free to rotate with respect to the piles. Each pile has 1.5% longitudinal steel ratio. The connection between the piles and the pile cap is described later in this section. This design uses a pin connection between the columns and the deck to prevent the formation of a flexural plastic hinge at the top of the column. To achieve similar level of displacements comparable to the FB bridge, the RPF design must incorporate a significant increase of the design strength because the RPF design results in significantly smaller hysteretic energy dissipation than that of the FB bridge. Furthermore, the use of pin connections between the columns and the deck used in the RPF designs reduce the stiffness and strength of the bridge compared to the FB design, especially in the longitudinal direction. Additional strength and

8

stiffness was achieved using larger foundations and columns as well as stiffer and stronger bearings at the abutments. Hysteretic energy dissipation was provided by using LPRBs in the abutments.

In this design the columns are designed to remain elastic for the maximum moment resistance of the foundation at the top of the piles. This resistance can be approximated to be equal to $W_{tot}B_D/2$, where W_{tot} is the vertical force at the top of the piles and B_D the distance between the outer face of the two piles along the diagonal [see Figure 2(e)]. The bending moment resistance due to friction between the vertical sides of the pile-cap and the soil is ignored. The pile cap is 8.8 m × 7.2 m × 2.4 m and 8.5 m × 7.0 m × 2.4 m for the RPF17 and RPF8 bridges, respectively. The piles—1.5 m in diameter and 25 m long—protrude 0.8 m into the pile cap, see Figure 2(f) and (g).

The protruding part of the piles into the pile cap is wrapped with a 60 mm thick neoprene sheet with shear modulus of neoprene used here $G_n = 0.03$ MPa. The pile cap seats on the piles without any tension force transfer connection other than the shear force that can be transferred from the pile cap to the neoprene wrap. A 30 mm thick 1.5 m diameter rubber pad with $G_r = 0.6$ MPa is used between the top of the piles and the pile cap, see Figure 2(g) and (h). Neoprene wraps are used to achieve a smoother contact and normal force transfer between the pile cap and the piles while allowing nearly free uplift and rotation of the pile cap. The rubber pads at the top of the piles are used in order to achieve small horizontal displacements of the pile cap in respect to the piles and help engage all four piles in shear. Both the neoprene wraps and the rubber pads are glued to the piles. In addition, an 80 mm-thick foam layer is used at the base of the pile cap to prevent unintended overstrength due to vertical resistance of the soil underneath the pile cap.

Each pile is designed to resist the entire gravity force the pile cap caries by utilizing the shaft resistance, Q_s, of the pile and about 20% of base resistance, Q_b. For sand with representative angle of friction $\varphi' = 39^o$ and the pile geometry used here, $Q_s = 6.6$ MN and $Q_b = 39$ MN (Fleming et al. 2009). The water table was assumed to be 11 m below the ground surface. Based on lateral capacity analysis (Fleming et al. 2009), each pile for zero and 14.5 MN axial load can resist 2.5 MN and 2.8 MN of lateral force, respectively. The lateral capacity was calculated at the point where the longitudinal tension strain in the pile reaches 0.5%. The column in the RPF bridges was 2.5 m in diameter with 3% longitudinal steel ratio along the entire column height. For 11.1 MN axial load, the nominal flexural strength of the column was computed based on moment curvature section analysis equal to 54 MN-m.

Bridges with rocking shallow foundations (RSF)

The soil near the ground surface for bridges RSF17 and RSF8 is assumed to have $\varphi'=37^o$ and specific weight $\gamma = 18.6$ kN / m^3. The response objectives in this case were identical to those for the RPF designs. The length and the depth of the square footings are equal to 8.0 m and 2.0 m, respectively, for both RSF17 and RSF8 bridges, while the embedment depth is 0.5 m. For these soil properties and geometry of the footings and 13.9 MN vertical force the bearing stress capacity is $q_{bl} = 2.6$ MPa (Meyerhof 1963), resulting in a vertical force factor of safety $FS_v = 12$. The maximum moment capacity of the footing is calculated to be $M_{max} = 52$ MN-m; the corresponding length of the contact area between the soil and the footing at M_{max} is $0.17B_T$. The columns of bridges RSF17 and RSF8 are identical to those of bridges RPF17 and RPF8, respectively.

Numerical Model

The analyses were conducted using the Open System for Earthquake Engineering Simulation (OpenSees, 2012) computer software. Figure 4(a) shows the 3D model. Nonlinear fiber-section Euler Bernoulli beam-column elements were used to model the columns and the deck. For each of the columns, two beam elements of equal length were used, with 5 and 4 integration points each for the 17 m and 8 m tall bridges, respectively. Two beam elements, with three integration points each, modeled each span of the deck. The material models *Concrete03* and *Steel02* were used to model the concrete and reinforcing steel, respectively, in each of the nonlinear beam-column elements. Expected values of material properties were used. The expected compressive strength of the concrete used was $f_{c,e} = 62$ MPa, and the yield stress of the steel was $f_y = 455$ MPa with a 2% hardening ratio. The expected compressive strength of the confined concrete of the columns was $f_{cc,e} = 80$ MPa. The initial post-tensioning force of the deck was modeled using the initial strain material. The strands were modeled with fibers having the *Steel02* material behavior and yield strength $f_{ps,y} = 1670$ MPa. Linear elastic stiff elements connected the top and bottom of the columns with the centroid of the deck and the foundation centroid, respectively, as well as the centroid of the foundation to the bottom of the foundation, see Figure 4(b). At the interface of column with the top of the foundation and the base of the deck, a zero-length-section element modeled the strain penetration of the longitudinal reinforcement of the column in the foundation and the deck, respectively. The sections of these zero-length elements were identical to these of the beam elements of the columns and used the same materials, but the tangent modulus of the

materials was 17 times smaller. The P-Delta geometric transformation was used for all the beam elements. The columns of the FB bridges were modeled as fixed at their base.
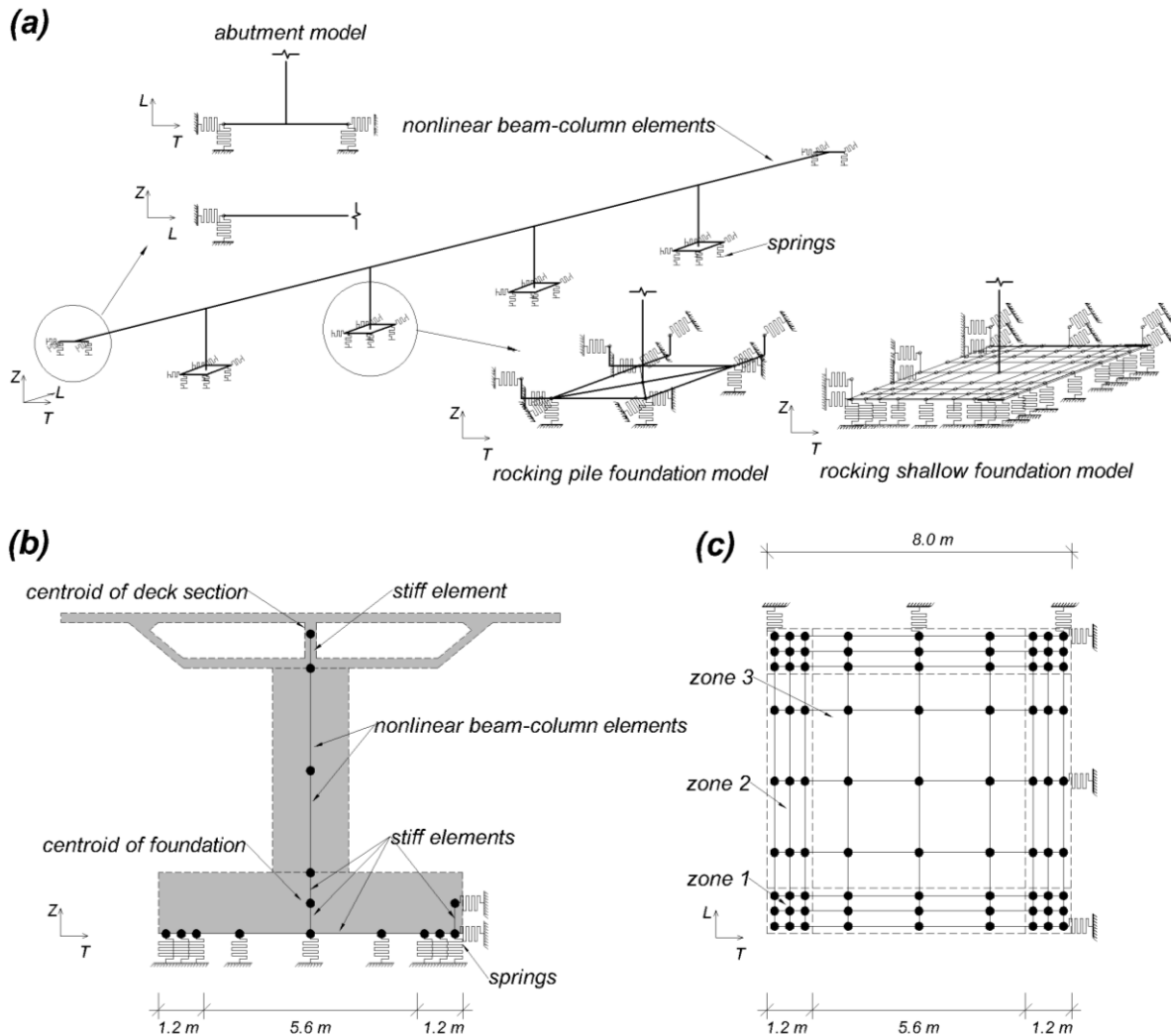

Figure 4. Schematic of the numerical model: (a) three dimensional view; (b) elevation section view of the foundation, column and deck of bridge RSF8; and (c) plan view of the model of the rocking shallow foundations.

Spring elements modeled the rubber bearings at the abutments. For each bearing, two horizontal springs (one in the longitudinal and another in the transverse direction) and one vertical spring were used. The rubber bearings of the FB bridges were modeled as linear in the horizontal directions with stiffness $K_h = 0.85$ MN /m. In the vertical direction, the bearings were modeled to have a linear behavior with stiffness $K_{v,c} = 795$ MN/m, and $K_{v,t} =$

79.5 MN/m in compression and tension, respectively. The LPRBs were modeled to have a bilinear force-displacement (F-Δ) relation with initial stiffness of 30.8 MN / m, post-yield stiffness equal to 2.4 MN/m, and a yield force equal to 0.9 MN. For these bearings $K_{v,c}$ = 8750 MN/m and $K_{v,t}$ = 875 MN/m.

The combined behavior of expansion joint, abutment wall and the backfill soil were modeled in the longitudinal direction using a spring with zero tensile strength and a bi-linear behavior with gap in compression [see Figure 5(a)]. The shear keys were modeled using spring elements in the transverse direction with the tri-linear force-displacement relationship shown in Figure 5(b).
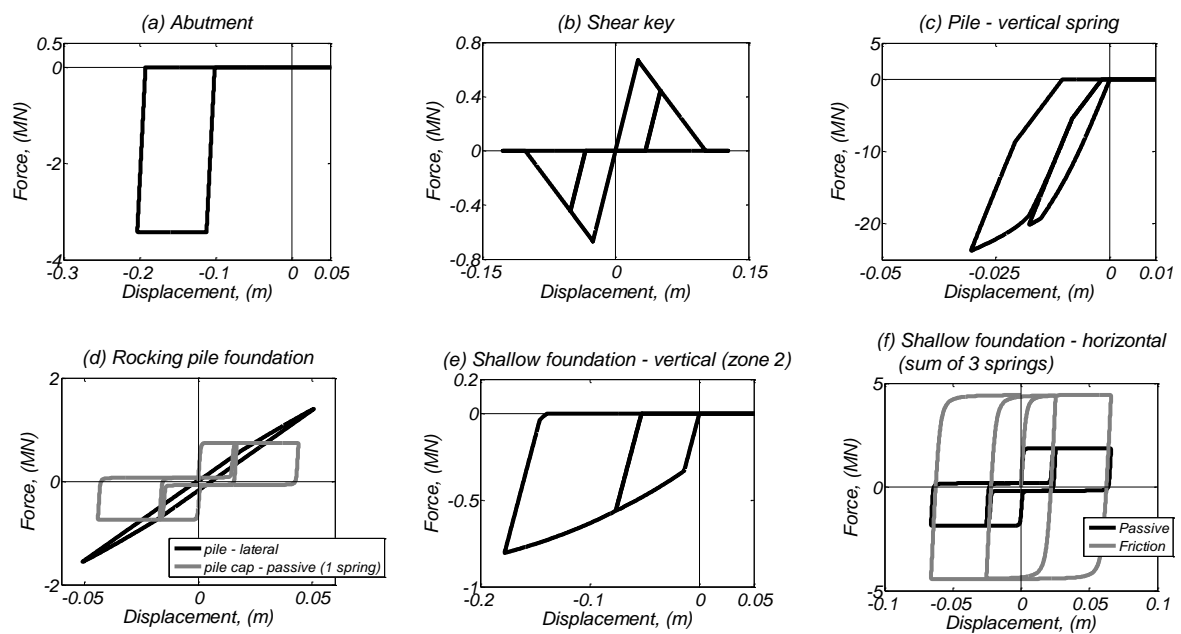

Figure 5. Force-displacement relations of the different springs used in the bridge models for different components.

The behavior of each pile of the rocking pile foundations in the vertical direction was modeled using a spring located at the centroid of the pile. This spring had zero tensile strength and the nonlinear F-Δ behavior shown in Figure 5(c), the result of using in parallel *QzSimple1* the *TzSimple1* materials (OpenSees, 2012) to model the bearing and shaft behavior, respectively, of the pile. Springs having the *PySimple1* nonlinear F-Δ relation shown in Figure 5(d) were used to model the lateral F-Δ behavior of each pile. The passive pressure from the soil to the sides of the pile cap was modeled with two springs, see Figure 4(a), in each of the longitudinal and transverse direction, with the nonlinear *PySimple1* F-Δ relation shown in Figure 5(d). The friction between the four vertical sides of the pile cap and

the soil was ignored in the model. The neoprene wraps around the top of the piles as well as the rubber pads at the top of the piles were not modeled.

The soil underneath each shallow foundation was modeled using 81 springs; see Figure 4(b) and (c). The vertical force-displacement relation was modeled using the *QzSimple1*-type 2 *F-Δ* relation shown in Figure 5(e). In terms of *F-Δ* relation of these springs, three zones were distinguished [see Figure 4(c)]. The control parameters of the *F-Δ* relation for these springs in each of the three zones are listed in Table 3 as follows: (a) the area each spring represents; (b) the ultimate soil stress, q_u; and (c) the secant stiffness, K_z, at 50% of ultimate force of the spring. The q_u of the springs of zones 1 and 2 is determined accounting for the contact area between the foundation and the soil (Meyerhof 1963) at maximum moment resistance of the foundation. The K_z was determined according to the recommendations of Harden and Hutchinson (2009). The passive resistance of the soil on the vertical sides of the foundation was modeled using three springs, in each of the longitudinal and transverse directions, see Figure 4(a) and (c), having the *PySimple1* F-Δ relation shown in Figure 5(f). The friction resistance at the base of the shallow foundation was modeled using three springs, in each of the longitudinal and transverse directions, having the *Tzsimple1* nonlinear F-Δ relation [see Figure 5(f)]. For both the shallow foundations and the pile caps a grid of linear stiff beam elements modeled the perimeter and connected it with the centroid. For all six bridge models studied, aspects of the soil-foundation-superstructure interaction—such as radiation damping as well as the response of the soil beyond that in the immediate vicinity of the shallow foundations—were ignored.

Translational and rotatory masses were lumped at the nodes of the deck, the nodes at the mid-height of the columns, and the nodes at the centroid of the foundations. Uniformly distributed gravity forces were assigned along the deck. Point gravity forces were assigned at the middle and base of the columns and the centroid of the foundations. Mass and initial stiffness proportionate Rayleigh damping was used with 2% damping ratio in the following two modes: the first mode with the predominant translational component in the transverse direction and the first mode with the predominant translational component in the longitudinal direction.

Table 3. Main characteristics of springs modeling the soil beneath the shallow foundations. Zones 1 to 3 are shown in Figure 4(c).

	Area (m^2)	Ultimate stress, q_{bl}, (MPa)	Secant stiffness per unit area at 50% of ultimate stress, K_z, (MN/m/m^2)
Zone 1 (end-end)	0.16	1.47	11.6
Zone 2 (mid-end)	0.75	1.47	11.5
Zone 3 (mid-mid)	3.48	2.59	0.27

Analysis Results

Modal Analysis and Monotonic Static Analysis Results

Table 4 shows the two modal periods of the six bridges with the most predominant translational component in the transverse ($T_{1,T}$) and longitudinal ($T_{1,L}$) direction, respectively, computed using initial stiffness properties for all the elements. Figure 6 plots the results of the monotonic static analysis in the transverse and the longitudinal direction in terms of total force versus column drift ratio in the corresponding direction for all six bridges using the corresponding modal force vector computed with the modal analysis described above. The column drift ratio is defined here as the relative displacement in a specific direction of the node at the deck centroid above the column of interest to the height of this node from the top of the foundation for the FB bridges, from the top of the piles for the RPF bridges and from the bottom of the foundation for the RSF bridges.

Table 4. Modal periods for the main mode in transverse and longitudinal direction of the six bridges.

	FB17	RPF17	RSF17	FB8	RPF8	RSF8
$T_{1,T}$, (s)	1.25	0.83	1.15	0.45	0.40	0.62
$T_{1,L}$, (s)	0.71	0.88	0.94	0.31	0.54	0.61

The monotonic static analysis results indicate the expected major differences in initial stiffness and strength of the bridges in the transverse direction. At 4% column drift ratio in the transverse direction, bridge RPF17 and RSF17 have 1.7 times the strength bridge FB17; Note the significantly higher initial stiffness of bridge RPF17 compared to that of bridges FB17 and RSF17. Regarding the 8 m tall bridges, bridges RPF8 and RSF8 have 1.5 and 1.6

times, respectively the strength of bridge FB8 at 3% drift ratio while the initial stiffness of bridge RPF8 is significantly higher than that of bridges FB8 and RSF8.

The pushover analysis in the longitudinal direction shows that the three 17 m tall bridges have similar behavior up to 4% drift ratio. For the 8 m tall bridges, bridge FB8 has the highest initial stiffness as well as strength for any drift ratio.

Based on the pushover analysis results, the column axial compression force increase in the exterior column at 4% column drift ratio in the transverse direction was less than 0.4 MN for all bridges. As described in the next section, note that this value is significantly smaller than the level of column compression force increase computed with response history analysis. This is primarily because the static pushover analysis does not account for the vertical inertia effects. Note that the vertical component of the excitation is not used here.
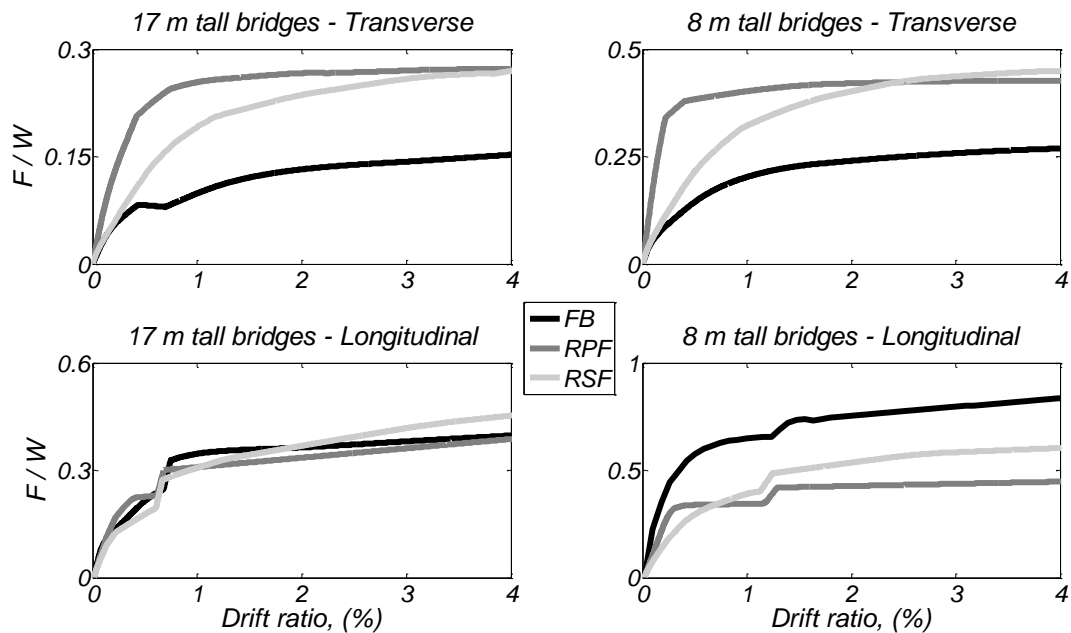

Figure 6. Force-displacement response of the six bridges based on a pushover analysis: (top row) in the transverse direction; (bottom row) in the longitudinal direction. Left column shows the results for the 17 m tall bridges and right column for the 8 m tall bridges.

Mean Response History Analysis Results for the Fourteen Scaled Ground Motions

Presented below are the results of nonlinear response history analysis to the sets of 14 ground motions. For each set of ground motions scaled at the DE and MCE level of shaking, two analyses cases were performed: (1) the first analysis considered the fault-normal and fault-parallel component parallel to the transverse, and longitudinal direction, respectively, of the

bridges, termed the FNT case; and (2) the second analysis considered the fault-normal and fault-parallel component parallel with the longitudinal and transverse axis, respectively, of the bridges, termed the FNL case. The arithmetic mean results of specific response parameters for the FNT and FNL analyses are listed in Table 5 and 6, respectively.

Results for both the DE and MCE level of shaking are presented in each of these tables. The displacement response parameters listed in these tables are as follows: (a) the column (peak among all four columns) drift ratio at any horizontal direction; (b) the residual column drift ratio (only for the FNT analysis case); (c) the displacement of the expansion joint in the longitudinal direction; (d) the peak displacement of the bearings at the abutments in any horizontal direction; (e) the peak settlement in any of the piles of the rocking pile-foundations; and (f) the peak settlement computed in any of the springs under the shallow foundations. Other response parameters provided are the tension strain of the longitudinal reinforcement at the base and at the top of the exterior and interior columns as well as the peak longitudinal tension strain of the deck along its entire length. As reported, the tensile strain of the deck is the total strain. Lastly, these tables list the compression axial force increase $\Delta P_c/P_g$ in both the columns where ΔP_c is the difference between the peak axial compression force computed in a column and the compression force due to gravity P_g. The compression axial force increase of the columns is calculated after filtering out the computed axial force history to eliminate spurious spikes related to the type of the nonlinear material and F-Δ relations used here (Wiebe and Christopoulos 2010). A low-pass finite impulse response filter in MATLAB of order equal to 5000 is used. The ΔP_c for two different cut-off frequencies—10 Hz and 5 Hz—are reported.

Table 5. Mean response parameters for the six bridges subjected to the 14 ground motions scaled at the DE and MCE, in parenthesis, level of shaking for case FNT.

		FB17	RPF17	RSF17	FB8	RPF8	RSF8
	Column drift ratio, (%)	2.81 (4.89)	2.29 (4.07)	2.54 (3.99)	2.28 (3.60)	3.10 (4.56)	3.43 (4.96)
	Residual drift ratio, (%)	0.08 (0.15)	0.01 (0.01)	0.06 (0.17)	0.06 (0.07)	0.03 (0.07)	0.08 (0.16)
	Expansion joint displ., (m)	0.20 (0.30)	0.20 (0.33)	0.19 (0.29)	0.05 (0.08)	0.13 (0.25)	0.14 (0.25)
	Bearing displ., (m)	0.44 (0.72)	0.24 (0.39)	0.23 (0.39)	0.22 (0.31)	0.18 (0.32)	0.19 (0.31)
	Pile settlement, (mm)	N/A	17 (21)	N/A	N/A	27 (38)	N/A
	Foundation settlement, (m)	N/A	N/A	0.12 (0.17)	N/A	N/A	0.16 (0.22)
Longitudinal reinforcement tensile strain	Interior column base (%)	3.29 (5.01)	0.18 (0.21)	0.11 (0.13)	3.55 (5.18)	0.21 (0.32)	0.09 (0.11)
	Exterior column base (%)	3.44 (5.30)	0.16 (0.18)	0.09 (0.12)	3.96 (5.57)	0.15 (0.20)	0.08 (0.10)
	Interior column top (%)	1.63 (2.83)	N/A	N/A	1.56 (2.93)	N/A	N/A
	Exterior column top (%)	1.63 (2.83)	N/A	N/A	1.47 (2.71)	N/A	N/A
Column axial compression force increase	Interior col., (10 Hz)	0.16 (0.21)	0.64 (0.88)	0.36 (0.40)	0.34 (0.44)	1.57 (1.80)	0.84 (1.02)
	Exterior col., (10Hz)	0.17 (0.21)	0.39 (0.56)	0.24 (0.32)	0.42 (0.48)	1.06 (1.37)	0.61 (0.78)
	Interior col., (5 Hz)	0.16 (0.21)	0.50 (0.65)	0.34 (0.39)	0.33 (0.42)	1.06 (1.29)	0.79 (0.96)
	Exterior col., (5Hz)	0.17 (0.21)	0.33 (0.48)	0.22 (0.31)	0.40 (0.47)	0.79 (0.96)	0.58 (0.74)
	Deck tensile strain, (%)	0.02 (0.05)	0.16 (0.23)	0.16 (0.22)	0.05 (0.08)	0.17 (0.25)	0.18 (0.27)

Table 6. Mean response parameters for the six bridges subjected to the 14 ground motions scaled at the DE and MCE, in parenthesis, level of shaking for case FNL.

		FB17	RPF17	RSF17	FB8	RPF8	RSF8
	Column drift ratio, (%)	2.17 (3.24)	2.15 (3.56)	2.16 (3.29)	1.92 (3.16)	3.01 (4.44)	3.38 (4.99)
	Expansion joint displ., (m)	0.26 (0.42)	0.28 (0.49)	0.27 (0.46)	0.09 (0.16)	0.26 (0.37)	0.25 (0.37)
	Bearing displ., (m)	0.35 (0.53)	0.30 (0.51)	0.29 (0.48)	0.17 (0.27)	0.27 (0.38)	0.26 (0.38)
	Foundation settlement, (m)	N/A	N/A	0.11 (0.17)	N/A	N/A	0.16 (0.23)
Longitudinal reinforcement tensile strain	Interior column base (%)	3.19 (4.68)	0.19 (0.22)	0.12 (0.12)	4.31 (6.37)	0.16 (0.21)	0.09 (0.11)
	Exterior column base (%)	3.24 (4.74)	0.16 (0.19)	0.10 (0.12)	4.56 (6.60)	0.14 (0.17)	0.08 (0.10)
	Interior column top (%)	2.65 (4.23)	N/A	N/A	3.43 (5.44)	N/A	N/A
	Exterior column top (%)	2.65 (4.23)	N/A	N/A	3.38 (5.43)	N/A	N/A
Column axial compression force increase	Interior col., (10 Hz)	0.25 (0.26)	0.59 (0.73)	0.34 (0.43)	0.50 (0.60)	1.18 (1.47)	0.82 (1.06)
	Exterior col., (10Hz)	0.26 (0.29)	0.38 (0.57)	0.25 (0.35)	0.50 (0.61)	0.92 (1.18)	0.61 (0.85)
	Interior col., (5 Hz)	0.23 (0.25)	0.46 (0.58)	0.33 (0.41)	0.43 (0.54)	0.82 (1.08)	0.78 (0.99)
	Exterior col., (5Hz)	0.24 (0.28)	0.33 (0.46)	0.24 (0.32)	0.44 (0.55)	0.64 (0.91)	0.60 (0.82)
	Deck tensile strain, (%)	0.02 (0.03)	0.13 (0.20)	0.11 (0.18)	0.05 (0.08)	0.12 (0.20)	0.14 (0.23)

Results for the case with fault-normal component in the transverse direction (FNT)

First the response of the 17 m tall bridges (FB17, RPF17, RSF17) is discussed. The drift ratio of the FB, RPF, and RSF bridges was 2.81%, 2.29%, and 2.54%, respectively, at the DE level of shaking. The corresponding values at the MCE level of shaking were 4.89%, 4.07%, and 3.99%, respectively. Note that the rocking foundation designs for the 17 m tall bridges resulted in drift ratios about 0.81 to 0.90 times that of the FB bridge for both levels of excitation. The expansion joint displacement of bridge FB17 was 0.20 m and 0.30 m at the DE and MCE levels of shaking, respectively. In the longitudinal direction (at both these levels of displacement) the expansion joint displacement capacity was exceeded and the passive resistance of soil in the abutment was fully mobilized; the approach slab has possibly been completely damaged. Similar was the level of response of the expansion joints and of backfill in the abutments in bridges RFP17 and RSF17. Bridge FB17 developed 0.44 m and 0.72 m displacement of the bearings at the DE and MCE level of shaking, respectively. Bridges RPF17 and RSF17 experienced displacement of the rubber bearings less than 0.39 m at the MCE level of shaking, remaining undamaged. The significantly larger stiffness and strength of the LPRBs were key in reducing the displacement of the bearings in bridges RPF17 and RSF17 compared to bridge FB17.

Figure 7 (a) and (b) plot the instantaneous displacement, in the transverse direction, of the 17 m tall and 8 m tall bridges, respectively, for the FNT analysis case when the interior column drift ratio was 4%. The profiles reported are the arithmetic mean profiles for the ground motions where the column drift ratio reached 4%. The displacement profiles of the bridges with rocking foundations was significantly different than that of the fixed-base bridges having a more curved shape due to the smaller displacements in transverse displacement in the abutments. This difference in displacement in the transverse directions between the abutments and the columns results in bending of the deck and should be explicitly considered during the design to prevent damage of the post-tension strands. Here the characteristics of the columns and of the LPRBs were designed so that the deck remained nominally elastic and the post-tensioned strands elastic and undamaged.
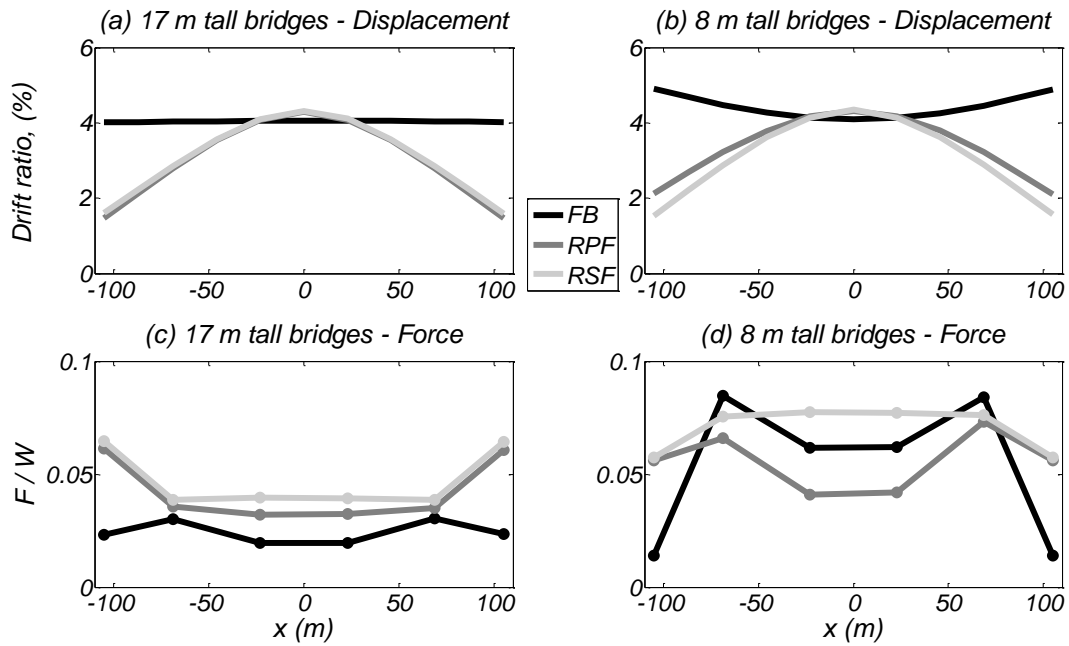
Figure 7. Instantaneous profile of drift ratio and total lateral resisting force in the transverse direction of the bridges at 4% drift ratio of the interior column (when the column experiences it for first time). The profiles are the arithmetic mean profiles computed for the ground motions (6 to 10 motions out of the 14 for the FNT analysis case) where interior column drift ratio reaches 4%. At the mid-length of the deck x = 0 m.

Figure 7(c) and (d) plot the shear force in the transverse direction along the length of the bridges at the same instants to those described in Figure 7(a) and (b), respectively. The shear force along the bridge is more uniform for bridge FB17 compared to the profile of shear force in bridges with the rocking foundations. This is because of the effect of the LPRBs in bridges RPF17 and RSF17, which resulted in larger shear force at the abutments.

The bridges with rocking foundations resulted in elastic response of the columns, with the tension strain less than 0.21% at the MCE level of shaking. The deck remained nominally elastic with longitudinal tension strain equal to 0.23% at the MCE. The total strain in the strands for this level total deck strain is 0.8%. For this level of tensile strain the strands remain elastic and undamaged (Veletzos and Restrepo 2011). For bridge RSF17, the settlement of the shallow foundations was 0.12 m, and 0.17 m at the DE and MCE level of shaking. Figure 8(a) and (b) show the computed moment versus rotation, *M-θ*, of the shallow foundation in the transverse direction of bridge RSF17 and RSF8, respectively, for one of the 14 ground motions used scaled at the MCE level of shaking. The *M-θ* for both these bridges shows less than 0.7% rotation when passing from zero moment up to 6.6% foundation rotation. While the column residual drift ratio bridges RPF17 was practically zero, bridge

RSF17 experienced 0.17% residual drift ratio at the MCE level of shaking. The vertical displacement of the piles of bridge RPF17 reached 38 mm at the MCE level of shaking, as shown in Table .

Bridge FB17, however, developed significant inelastic deformations in the columns, especially at their base, with the strains that reached 3.44%, and 5.30% at the DE and MCE level of shaking, respectively. At both these levels of inelastic deformation extensive spalling of concrete in the flexural plastic hinges should be expected while longitudinal reinforcement bar buckling may occur at the MCE level of shaking. The residual drift ratio of bridge FB17 was small and equal to 0.15% at the MCE levels of shaking.

The difference in the level of inelastic response between bridges FB17 and RPF17 is shown in Figure 9, which plots the total shear force in the transverse direction of the bridges versus column drift ratio for one of 14 ground motions scaled to the MCE level of shaking. This figure shows the smaller extent of inelastic response that occurs in bridge RPF17, mainly due to inelastic behavior of the lead-plug of the LPRBs.

The axial compression force increase, ΔP_c, (for a 10 Hz cut-off frequency) in the columns of the FB17 and the RSF17 reached 0.21 and 0.40, respectively, at the MCE hazard level of shaking. This increase is due to framing between the columns the deck and the abutment, and vertical inertia effects. The axial compression force variation was significantly higher in bridge RPF17, reaching 0.64 and 0.88 at the DE and MCE levels of shaking, respectively. This larger magnitude of axial compression force increase is due to the greater regain of stiffness that occurs in the RPF bridges upon contact of the pile cap to the piles compared to the other two bridge designs.
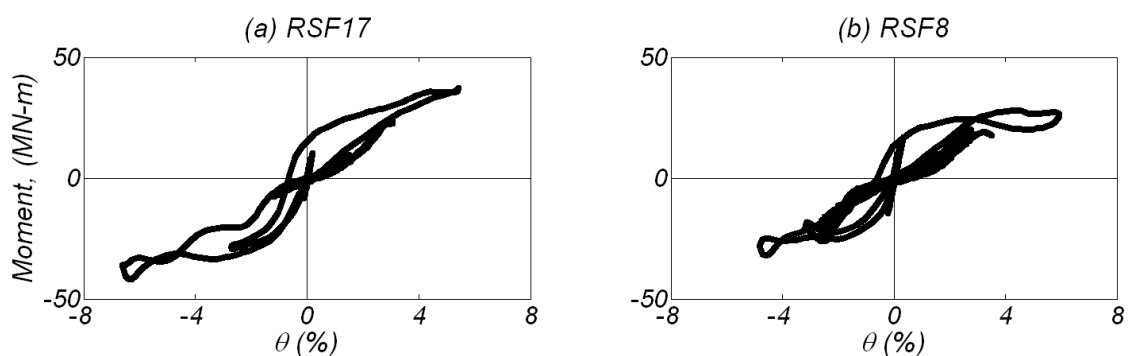

Figure 8. Moment-rotation response of shallow foundation of interior column of bridges RSF17 and RSF8 for one of the 14 ground motions scaled at MCE.
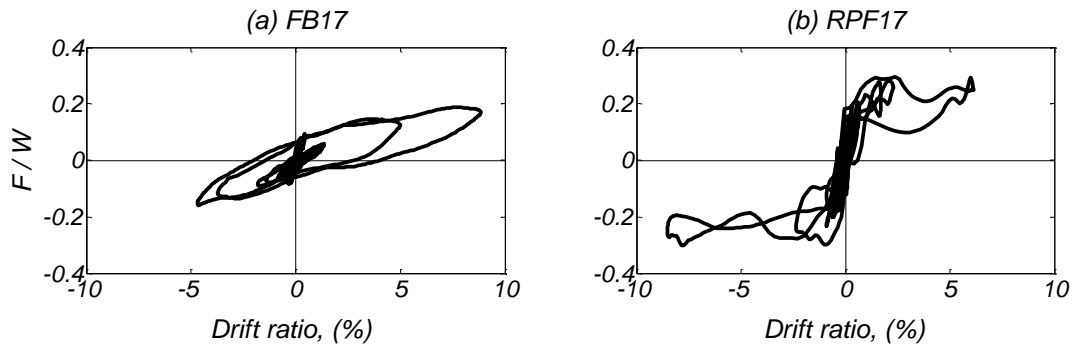
Figure 9. Total resisting force (columns, bearings, shear keys) in the transverse direction versus column drift ratio for bridges FB17 and RFP17 for one (different for each bridge) of the 14 ground motions scaled at the MCE.

Next, the response of the 8 m tall bridges (FB8, RPF8, and RSF8) is discussed. In contrast to the behavior of the 17 m tall bridges, bridges RPF8 and RSF8 experienced significantly higher levels of displacements compared to bridge FB8 at both the DE and MCE levels of shaking. While the drift for bridge FB8 was 2.28% and 3.60% at the DE and MCE level of shaking, respectively, for bridges RPF8, and RSF8 the drift ratio ranged between 3.10% and 3.43%, respectively, at the DE .The corresponding numbers for the MCE level were 4.56% and 4.96%. This is because the effect of reduced hysteretic energy dissipation (elastic columns on rocking foundations) on the level of increase of nonlinear displacement compared to that of columns that develop plastic hinges, increases with decrease of the structural period (Antonellis and Panagiotou 2013) for initial periods 0.5 to 2 s.

Despite the larger drift ratio, the bridges with rocking foundations (RSF8 and RPF8) did not experience inelastic deformations in the columns, with tensile longitudinal strain less than 0.32% at the MCE level of shaking. Bridge RSF8 resulted in soil settlements equal to 0.16 m and 0.22 m at the DE and MCE level of shaking, respectively. Figure 8(b) shows the computed moment rotation of the shallow foundation of bridge RSF8 for one ground motion. The deck remained nominally elastic for both bridges RPF8 and RSF8, with less than 0.27% tension longitudinal strain at the MCE level of shaking. The corresponding total strain in the strands was 0.8%. Bridge FB8 however, experienced significant inelastic deformations in the columns, especially at their base, with longitudinal tension strains reaching 3.96%, and 5.57% at the DE and MCE level of shaking, respectively. The residual drift ratio at MCE level of shaking of bridges FB8, RP8, and RS8 were small and less than 0.16%.

The 8 m tall bridges experienced about two times the axial compression force increase, ΔP_c, of the 17 m tall bridges due to larger vertical inertia effects. The column axial force compression increase in bridges FB8 and RSF8 reached 0.42, and 0.84, respectively, at

the DE level of shaking. The corresponding values at the MCE level of shaking were 0.48, and 1.02, respectively. Bridge RPF8 experienced significantly higher ΔP_c, which was 1.57 and 1.80 at the DE and MCE level of shaking, respectively. Note that the corresponding values for 5 Hz cut-off frequency reduced to 1.06 and 1.29, indicating that this increase in axial load increase is significant in frequencies between 5 and 10 Hz. For the FB and RSF bridges negligible differences in ΔP_c occurred for the 5 Hz and 10 Hz cut-off frequencies demonstrating that ΔP_c was rich in frequencies lower than 5 Hz.

Results for the FNL analysis case

Compared to the FNT case, the FNL analysis case resulted in larger responses for the expansion joint displacements, the displacement of the bearings of the bridges with rocking foundations, the column tension strains for bridge FB8, especially at the top, and in some cases for the column axial compression force increase for the fixed-base bridges. Bridge FB17 reached 0.26 m, and 0.42 m displacement of the expansion joints at the DE and MCE level of shaking, respectively. The corresponding values for bridges RPF17 and RSF17 were 0.28 m and 0.49 m. Both bridges FB17 and FB8 developed significant inelastic response in the columns with the tension strain of the longitudinal reinforcement reaching 3.24%, and 4.56%, respectively at the DE level of shaking. The corresponding values of strain at the MCE level of shaking were 4.74%, and 6.60%. Note that the tensile strains at the top of the columns are significantly higher for the FNL case for bridges FB17 and FB8, reaching 4.23% and 5.44% at the MCE level, respectively. For bridges FB17 and FB8 the column axial compression force increase ΔP_c was up to 1.38 times (bridge FB17) that of the FNT case.

Conclusions

We investigated numerically the seismic response of six reinforced concrete bridges located in Oakland, California, 3 km from the Hayward fault. All bridges were 210 m long, linear, and had 5 spans. Three of the bridges analyzed were 17 m tall and three were 8 m tall. For each bridge height, three designs of columns and foundations were studied: (a) a conventional bridge designed according to Caltrans seismic design criteria that is expected to develop flexural plastic hinges in columns fixed to pile foundations and the foundation fixed to the ground; (b) columns designed to remain nominally elastic and fixed on rocking pile foundations; and (c) columns designed to remain nominally elastic and fixed to rocking shallow foundations.

The columns used in the bridges with rocking foundations were 2.5 m in diameter with a 3% longitudinal steel ratio, ρ_l; the fixed-base bridges had 1.8 m diameter columns with $\rho_l = 2\%$. The pile cap of the rocking pile foundations had a volume 1.6 times that of the pile cap used in the fixed-base bridges. The columns of the bridges with rocking foundations used a pin connection between the column and the deck. In addition, the bridges with rocking foundations used 1.26 m diameter lead-plug rubber bearings at the abutments compared to 0.6 m diameter laminated rubber bearings used in the fixed-base bridges. Bridges RPF17 and RSF17 at 4% drift ratio in the transverse direction had 1.7 times the lateral strength of the fixed-base bridge. Bridges RPF8 and RSF8 at 4% drift ratio in the transverse direction had about 1.6 times the lateral strength of the fixed-base bridge. Three-dimensional nonlinear response history analyses were performed, using two components of horizontal excitation for a set of ground motions scaled to two seismic hazard levels with return periods of 975 [design earthquake (DE)] and 2475 years [maximum considered earthquake (MCE)], respectively. In one analysis case the fault-normal component of the motions was parallel to the transverse direction of the bridges (FNT case) and in the other case parallel to the longitudinal axis of the bridge (FNL case). Based on the results of the study the following conclusions are drawn:

1. The conventionally designed fixed-base bridges experienced significant inelastic deformations at both the DE and MCE levels of shaking. At the DE level of shaking the column drift ratio of bridges FB17 and FB8 was 2.81% and 2.28%, respectively. The corresponding values at the MCE level of shaking were 4.89% and 3.60%, respectively. At the DE level of shaking the tension strain of the longitudinal reinforcement of the columns of bridges FB17 and FB8 reached 3.44% and 4.56%, respectively. The corresponding values at the MCE level of shaking were 5.30% and 6.60%, respectively. For this level of inelastic deformation, extensive spalling of the concrete and possibly extensive yielding of the transverse reinforcement and buckling of the longitudinal rebars should be expected. The residual drift ratio at the MCE level of shaking of bridges FB17 and FB8 was small and less than 0.15%. The 17 m tall fixed-base bridge experienced 0.26 m, and 0.42 m of displacement in the longitudinal direction at the DE and MCE levels of shaking, respectively. This level of displacement exceeds the 0.1 m of displacement of the expansion joints and resulted in failure of the backwall in the abutments and the approach slab. The displacements of the bearings at the abutments were 0.44 and 0.72 m at the DE and MCE levels of shaking, respectively, with the latter to possibly exceed the deformation capacity of the bearings.

2.   Both the 17 m tall and 8 m tall bridges with rocking foundations resulted in nominally elastic response of the columns and the deck, while the post-tensioned strands remained elastic at both levels of shaking. Bridges RPF17 and RSF17 developed column drift ratios up to 0.83 times that of bridge FB17 in the FNT case. Bridges RPF8 and RSF8 developed drift ratios up to 1.4 times those of bridge FB8. The level of increase of nonlinear displacements for a bridge with columns on rocking foundations compared to that of a bridge designed to develop flexural plastic hinges in the columns should be expected to increase with decrease of structural period (for periods between 0.5 and 2 s). The residual column drift ratio of the bridges with rocking pile foundations was less than 0.07% and that of the bridges with rocking shallow foundations less than 0.17%. Inelastic response of the soil occurred at the ends of the rocking shallow foundations. For bridge RSF17 soil settlement reached 0.12 m, and 0.17 m (0.021 times the length of the foundation), respectively, at the DE and MCE level of shaking. The corresponding values for bridge RSF8 were 0.16 m and 0.23 m. The peak pile settlement of RPF was less than 40 mm at the MCE level of shaking. Bridges with rocking foundations developed displacements in the longitudinal direction which reached 0.49 m at the MCE level of shaking.

3.   The use of two large LPRBs at each abutment of these bridges was very effective in enhancing stiffness and strength, providing hysteretic energy dissipation, and thus controlling the level of displacements these bridges experienced. Differences in the strength and stiffness of the abutments and the columns resulted in bending of the deck in the transverse direction which should be explicitly considered in the analysis and design to ensure that the deck remains nominally elastic and that the strands do not yield.

4.   The bridges with rocking foundations experienced higher levels of column axial compression force increase, ΔP_c, than the fixed-base bridges. This increase is primarily due to vertical inertia effects and secondarily due to framing effects between the columns, the deck, and the abutments. The columns on rocking pile foundations experience the highest ΔP_c. This is because sudden regain of stiffness upon contact of the pile cap to the piles excites significant vertical oscillation and vertical inertia effects. Independent of the type of design ΔP_c of the 8 m tall bridges was 2 to 2.4 times that of the corresponding 17 m tall bridges. For bridge RPF8, ΔP_c reached 1.57 and 1.80 at the DE and MCE levels of shaking, respectively. The corresponding values for axial force histories filtered at 5 Hz were 1.06 and 1.29 indicating that these axial force histories were rich in high frequencies ranging between 5 Hz and 10 Hz. The ΔP_c of the fixed-base and RSF bridges was dominated by frequencies lower

than 5 Hz. This axial compression force increase should be explicitly considered in the design of the columns and the foundations.

References

Almond, J., and Kutter, B. L. (2012). "Design considerations for rocking foundations on unattached piles." *Journal for Geotechnical and Geoenviromental Engineering*, ASCE, submitted (under review).

Antonellis, G., and Panagiotou, M. (2013). "Seismic design and performance of bridges with columns on rocking foundations." *Pacific Earthquake Engineering Research Center Report*, Berkeley, CA (in press).

Apostolou, M., Gazetas, G., and Garini, E. (2007). "Seismic response of slender rigid structures with foundation uplift." *Soil Dynamics and Earthquake Engineering*, 27, 642-654.

Astaneh-Asl, H., and Roberts, J. (1996). "Seismic design, evaluation and retrofit of steel bridges." *Proceedings of the 2nd US Seminar*, San Francisco, USA.

Bartlett, P. E. (1976). "Foundation Rocking on a Clay Soil." M.E. thesis, University of Auckland.

Beck, J. L., and Skinner, R. I. (1974). "The seismic response of a reinforced concrete bridge pier designed to step." *Earthquake Engineering and Structural Dynamics*, 2, 343-358.

Caltrans Seismic Design Criteria version 1.6 (2010).

Chen, Y., Liao, W., Lee, C., and Wang, Y. (2006). "Seismic isolation of viaduct piers by means of a rocking mechanism." *Earthquake Engineering and Structural Dynamics*, 35, 713-736.

Chopra, A. K., and Yim S. C. (1985). "Simplified earthquake analysis of structures with foundation uplift." *Journal of Structural Engineering*, 111(4), 906-930.

Cormarck, L. G. (1988). "The design and construction of the major bridges on Mangaweka rail deviation." *The Institution of Professional Engineers of New Zealand*, 15(1).

Deng, L., Kutter, B. L., and Kunnath, S. K. (2012). "Probabilistic seismic performance of rocking- foundation and hinging-column bridges." *Earthquake Spectra*, 28(4), 1423-1446.

Deng, L., Kutter, B. L., and Kunnath, S. (2012). "Centrifuge modeling of bridge systems designed for rocking foundations." *Journal of Geotechnical and Geoenvironmental Engineering*, in press, DOI: 10.1061/(ASCE)GT.1943-5606.0000605.

Espinoza, A., and Mahin, S. A. (2008). "Shaking table and analytical investigation of reinforced concrete bridge piers with foundations allowed to uplift during earthquakes." *University of California at Berkeley*, Report No. UCB/SEMM-08/03.

Fleming, K., Weltman, A., Randolph, M., and Elson, K. (2009). "Piling Engineering.", third edition.

Gajan, S., Kutter, B. L., Phalen, J. D., Hutchinson, T.C., and Martin, G.R. (2005). "Centrifuge modeling of load-deformation behavior of rocking shallow foundations." Soil Dynamics and Earthquake Engineering, 25, 773-783.

Harden, C., and Hutchinson, T. (2009). "Beam-on-nonlinear-winkler-foundation modeling of shallow rocking-dominated footings." *Earthquake Spectra*, 25(2), 277-300.

Housner, G. H. (1963). "The behavior of inverted pendulum structures during earthquakes." *Bulletin of the Seismological Society of America*, 53(2), 403-417.

Kelly, J. M., and Tsztoo, D. F. (1977). "Earthquake simulation testing of a stepping frame with energy-absorbing devices." *University of California at Berkeley*, Report No. UCB/EERC-77/17.

Makris, N., and Zhang, J. (2001). "Rocking response of free-standing blocks under cycloidal pulses." *Journal of Engineering Mechanics*, 127(5), 473-483.

Matlab (2008). <http://www.mathworks.com/products/matlab/>

Mergos, P. E., and Kawashima, K. (2005). "Rocking isolation of a typical bridge pier on spread foundation." *Journal of Earthquake Engineering*, 9(2), 395-414.

Meyerhof, G. G. (1963). "Some recent research on the bearing capacity of foundations." *Canadian Geotechnical Journal*, 1(1), 16-26.

Milne, J., and Omori, F. (1893). "On the overturning and fracturing of brick and columns by horizontal applied motion." *Seismological Journal of Japan*, 17(1), 59-86.

Muto, K., Umemura, H., and Sonobe, Y. (1960). "Study of overturning vibration of slender structures." *Proc. 2nd. WCEE*, Tokyo, Japan, 2, 1239.

Negro, P., Paolucci, R., Pedretti, S., and Faccioli, E. (2000). "Large scale soil-structure interaction experiments on sand under cyclic loading." *Proc. 12th World Conference on Earthquake Engineering,* Auckland, New Zealand.

OpenSees (2012). <http://opensees.berkeley.edu/>

Paolucci, R., di Prisco, C., Vecchiotti, M., Shirato, M., and Yilmaz, M. T. (2007). "Seismic behavior of shallow foundations: large scale experiments vs. numerical modeling and implications for performance based design." *Proc. 1st US-Italy Seismic Bridge Workshop*, Pavia, Italy, April 19-20.

Pecker. A. (2006). "Enhanced seismic design of shallow foundations: example of the Rion Antirion bridge." *4th Athenian Lecture on Geotechnical Engineering*.

Pollino, M., and Bruneau, M. (2007). "Seismic retrofit of bridge steel truss piers using a controlled rocking approach." *Journal of Bridge Engineering*, ASCE, 12(5), 600-610.

Priestley, M. J. N., Evison, R. J., and Carr, A. J. (1978). "Seismic response of structures free to rock on their foundations." *Bulletin of the New Zealand National Society for Earthquake Engineering*, 11(3), 141-150.

Priestley, M. J. N., Seible, F., and Calvi, G. M. (1996). "Seismic design and retrofit of bridges."

Saidi, M., Gopalakrishnan, B. and, Siddharthan, R. (2002). "Shake table studies of effects of foundation flexibility on seismic demand in substandard bridge piers." *ACI Fifth International Conference*, Special Publication, SP-09, Cancun, Mexico, December 2002, 553-569.

Sakellaraki, D., and Kawashima, K. (2006). "Effectiveness of seismic rocking isolation of bridges based on shake table test." *First European Conference on Earthquake Engineering and Seismology*, Paper No. 364, Geneva, Switzerland.

USGS (2013). https://geohazards.usgs.gov/deaggint/2008/. Last time accessed March 2013.

Veletzos, M., and Restrepo, J. I. (2011). "Development of seismic design quidelines for segmental construction." *University of California at San Diego, La Jolla, CA*, Report no. SSRP-10/02,357-384.

Wiebe, L., and Christopoulos, C. (2010). "Characterizing acceleration spikes due to stiffness changes in nonlinear systems." *Earthquake Engineering and Structural Dynamics*, 39, 1653-1670.

Wiesing, P. R. (1979). "Foundation rocking on sand.", ME Thesis, Report No. 203, University of Auckland, School of Engineering. Auckland, New Zealand.

Wolf, J.P. (1976). "Soil-structure interaction with separation of base mat from soil (lifting-off)." *Nuclear Engineering and Design*, 38, 357-384.